

# Detection of neoplastic-immune hybrid cells with metastatic properties in uveal melanoma

**Ashley N. Anderson**

Oregon Health & Science University

**Patrick Conley**

Oregon Health & Science University

**Christopher D. Klocke**

Oregon Health & Science University

**Sidharth K. Sengupta**

Oregon Health & Science University

**Amara Pang**

Oregon Health & Science University

**Hannah C. Farley**

Oregon Health & Science University

**Abigail R. Gillingham**

Oregon Health & Science University

**Aubrey D. Dawson**

Oregon Health & Science University

**Yichen Fan**

Oregon Health & Science University

**Jocelyn A. Jones**

Oregon Health & Science University

**Summer L. Gibbs**

Oregon Health & Science University

**Alison H. Skalet**

Oregon Health & Science University

**Guanming Wu**

Oregon Health & Science University

**Melissa H. Wong** (✉ [wongme@ohsu.edu](mailto:wongme@ohsu.edu))

Oregon Health & Science University

---

Research Article

**Keywords:** uveal melanoma, metastasis, disseminated tumor cells, multiplexed cyclic immunofluorescence, single-cell RNA sequencing.

**Posted Date:** December 6th, 2023

**DOI:** <https://doi.org/10.21203/rs.3.rs-3694879/v1>

**License:**  This work is licensed under a Creative Commons Attribution 4.0 International License.

[Read Full License](#)

**Additional Declarations:** No competing interests reported.

---

# Abstract

## Background

Uveal melanoma is the most common non-cutaneous melanoma and is an intraocular malignancy affecting nearly 7,000 individuals per year worldwide. Of these, approximately 50% will progress to metastatic disease for which there are currently no effective therapies. Despite advances in molecular profiling and metastatic stratification of uveal melanoma tumors, little is known regarding their underlying biology of metastasis. Our group has identified a disseminated neoplastic cell population characterized by co-expression of immune and melanoma proteins, circulating hybrid cells (hybrids), in patients with uveal melanoma. Compared to circulating tumor cells, which lack expression of immune proteins, hybrids are detected at an increased prevalence in peripheral blood and can be used as a non-invasive biomarker to predict metastatic progression.

## Methods

To ascertain mechanisms underlying enhanced hybrid cell dissemination we identified hybrid cells within primary uveal melanoma tumors using single cell RNA sequencing and evaluated their gene expression and predicted ligand-receptor interactions in relation to other melanoma and immune cells within the primary tumor. We then verified expression of upregulated hybrid pathways within patient-matched tumor and peripheral blood hybrids using cyclic immunofluorescence and quantified their protein expression relative to other non-hybrid tumor and disseminated tumor cells.

## Results

Among the top upregulated genes and pathways in hybrid cells were those involved in enhanced cell motility and cytoskeletal rearrangement, immune evasion, and altered cellular metabolism. In patient-matched tumor and peripheral blood, we verified gene expression by examining concordant protein expression for each pathway category: TMSB10 (cell motility), CD74 (immune evasion) and GPX1 (metabolism). Both TMSB10 and GPX1 were expressed on significantly higher numbers of disseminated hybrid cells compared to circulating tumor cells, and CD74 and GPX1 were expressed on more disseminated hybrids than tumor-resident hybrids. Lastly, we identified that hybrid cells express ligand-receptor signaling pathways implicated in promoting metastasis including GAS6-AXL, CXCL12-CXCR4, LGALS9-P4HB and IGF1-IGFR1.

## Conclusion

These findings highlight the importance of TMSB10, GPX1 and CD74 for successful hybrid cell dissemination and survival in circulation. Our results contribute to the understanding of uveal melanoma tumor progression and interactions between tumor cells and immune cells in the tumor microenvironment that may promote metastasis.

## Background

Uveal melanoma (UM) is the most common primary intraocular cancer in adults and is associated with high rates of metastatic disease.(1, 2) Although there are low rates of detectable metastasis at diagnosis and treatment of primary UM is initially highly successful, nearly 50% of patients ultimately develop metastatic disease for which there is currently no curative therapy.(1–4) Presently, the risk for developing UM metastasis is most accurately estimated by gene expression profiling of the primary tumor, which classifies patients into two prognostic subgroups: classes 1 and 2, the latter of which carries increased risk for metastatic disease.(5) Despite significant advances in molecular prognostic tests for identifying patients at risk for developing UM metastases, the biological processes underlying UM metastasis remains poorly understood.

UM metastasizes almost exclusively via hematogenous spread, whereby tumor (or neoplastic) cells enter the circulation and primarily seed the liver.(6) Metastatic tumor growth requires a primary tumor cell to successfully navigate the metastatic cascade through dissemination, survival in circulation, extravasation, and colonization at the metastatic site. Identification and evaluation of neoplastic cells with high potential to disseminate and seed metastases is a critical step in understanding UM disease progression. One such cell type was recently identified by our laboratory as a neoplastic-immune hybrid cell population that shares genotypes and phenotypes from both immune and neoplastic cells.(7–9) In tumor-macrophage hybrid cells, these shared tumor and immune properties promote enhanced intravasation, migration, and seeding at distant metastatic sites in both colorectal and cutaneous melanoma hybrid cell lines.(7) In addition, cytoplasmic transfer of macrophage content to melanoma cells enhances tumor cell motility and dissemination.(10) The presence of hybrid cells in peripheral blood exposes an important relationship between the tumor and its immune microenvironment with implications on tumor progression.(8, 11) When hybrid cells are detected in peripheral blood, they are termed circulating hybrid cells (CHCs). CHCs are detected at substantially higher numbers than circulating tumor cells (CTCs) in patients with UM.(9) This is important as low levels of conventionally defined CTCs (those that lack the immune marker CD45) have limited use as a viable biomarker in patients with UM. Additionally, we have demonstrated that CHC levels predict metastatic progression in UM and have prognostic value for overall survival.(9) Hybrid cells have been identified in various primary tumor types(8, 12) and are detected in peripheral blood of patients with UM, however, their existence within primary UMs, as well as their distinct phenotypes as they relate to metastatic disease, remains to be determined.

In this study we sought to identify tumor-immune hybrid cells within UM primary tumors and evaluate hybrid cell phenotypes by combining highly multiplexed cyclic immunofluorescence (cyCIF) with analyses of a single cell RNA sequencing (scRNA-seq) dataset.(13) To initiate these studies, we developed a computational framework to validate hybrid cell identity within scRNA-seq as a single-cell population distinct from artifactual doublet cells commonly found in droplet-based sequencing methodologies. Our findings indicate that hybrid cells in UMs upregulate expression of genes established as core pathway mediators of cancer metastasis, including decreased cell adhesion and cytoskeletal rearrangements that

occur during cell invasion and migration, immune evasion pathways that allow tumor cells to escape immunogenic cell death, and metabolic pathways that have been shown to confer protection and promote enhanced survival in circulation and at metastatic sites.(14–16) Additionally, UM hybrid cells display upregulated expression of genes highly expressed in the liver, selenoprotein P1 (*SEPP1*) and glutathione peroxidase 1 (*GPX1*)(17, 18), highlighting a potential explanation for selective UM metastasis to the liver. We further verify that expression of three genes identified from our scRNA-seq analyses, thymosin beta 10 (*TMSB10*), *CD74* and *GPX1*, are expressed at the protein level in hybrid cells within patient-matched primary tumor and peripheral blood. Within disseminated cells in circulation, TMSB10 and GPX1 were expressed on a significantly higher number of CHCs compared to CTCs, highlighting the importance of these proteins in successful dissemination and a potential biomarker for UM disease progression. Lastly, we determined that hybrid cells retain key signaling pathways common in macrophages and in tumor cells, that can support their successful metastasis including growth arrest specific 6 – AXL receptor tyrosine kinase (GAS6-AXL)(19), C-X-C motif chemokine ligand 12 – C-X-C motif chemokine receptor 4 (CXCL12-CXCR4)(20), galectin 9 – prolyl 4-hydroxylase subunit beta (LGALS9-P4HB)(21) and insulin-like growth factor 1 – insulin like growth factor 1 receptor (IGF1-IGF1R)(22–25) which act to promote cancer cell invasion via actin remodeling, regulation of angiogenesis, and epithelial-mesenchymal transition (EMT). These findings contribute to our understanding of UM disease spread and provide evidence that hybrid cells possess critical metastatic features with potential to explain their increased prevalence in circulation.

## Methods

### Human specimens

All human formalin-fixed paraffin-embedded (FFPE) tissue samples and peripheral blood specimens were collected and analyzed in accordance with ethical requirements and regulations of the Oregon Health and Science University institutional review board. Informed consent was obtained from all subjects and studies were conducted under approved IRB protocol (IRB0005169). Single cell RNA sequencing of UM primary tumors was generated by collaborators at the University of Miami. (13) Sequencing data from this study was downloaded from the GEO entry GSE139829, available at

<https://www.ncbi.nlm.nih.gov/geo/query/acc.cgi?acc=GSE139829> .

The RAW data file (<https://www.ncbi.nlm.nih.gov/geo/download/?acc=GSE139829&format=file>) was utilized. The meta data for individual cells, including cell barcodes and annotated cell types, were directly provided by the original authors.

### Patient peripheral blood sample preparation

Peripheral blood (10mL) was collected from patients with UM at the time of diagnosis in heparinized vacutainer tubes (BD Biosciences, Franklin Lakes, NJ, USA) and diluted 1:2 with phosphate-buffered saline solution (PBS, 1.37 M NaCl, 27 mM KCl, 0.1 M Sodium phosphate dibasic, 18 mM KH<sub>2</sub>PO<sub>4</sub>, pH 7.4).

Peripheral blood mononuclear cells (PBMCs) were isolated using density centrifugation with Ficoll-Paque PLUS (GE Healthcare, Chicago, IL, USA) as previously published. (8) Isolated PBMCs were resuspended in buffer, then adhered to poly-D-lysine (1 mg/mL) coated slides (Millipore, Burlington, MA, USA; Fisher Scientific, Waltham, MA, USA) at 37°C for 15 min. Cells were fixed with 4% paraformaldehyde (PFA) for 5 min, permeabilized with 0.5% Triton-X (Fisher Scientific, BP151-100) for 10 min, and fixed again with 4% PFA for 10 min. After fixation, PBMC slides were then dehydrated in a series of ethanol baths (3 min each in 70%, 95%, and 100% ethanol) and stored at 4°C until used for immunofluorescent staining.

## Sample preparation and cyclic immunofluorescence

FFPE tissue sections (5 µm) from enucleated globes and patient matched isolated PBMC slides collected at the time of diagnosis were stained for melanocytic and immune markers using a flexible cyCIF method with oligonucleotide conjugated antibodies and directly labeled fluorescent primary antibodies as previously described (26–29) (n = 4). Briefly, tissue sections were deparaffinized with xylene and rehydrated with graded ethanol baths. Tissue was bleached for melanin removal in 10% H<sub>2</sub>O<sub>2</sub> for 20 min at 65°C. Antigen retrieval was performed using citrate buffer (Sigma-Aldrich, St. Louis, MO, pH 6.0) for 30 min at 100°C, washed for 1 minute in diH<sub>2</sub>O at 100°C, followed by Tris-HCl buffer (Invitrogen, Carlsbad, CA, pH 8.0), for 10 min at 100°C, then cooled to room temperature and washed with PBS (3 x 5 min). PBMC slides were prepared by 3 x 5 min washes in PBS. Tissue sections and PBMCs were then incubated with blocking buffer (PBS with 2.0% bovine serum albumin (BSA, bioWORLD, Dublin, OH), 0.05 mg/mL salmon sperm DNA (Thermo Fisher Scientific, Waltham, MA), and 0.5% dextran sulfate (Sigma-Aldrich, St. Louis, MO) for 30 mins at room temperature. Antibodies (**Supplemental Table 1**) in blocking buffer were applied overnight at 4°C in a humid chamber, followed by 3 x 5 min washes in 2X saline sodium citrate (SSC, BD Biosciences, Franklin Lakes, NJ, pH 7.0). Detection methods varied based on antibody type and round of staining (**Supplemental Table 1**), using either oligonucleotide conjugated secondary antibodies + imaging strands (IS) (27) (GPX1, TMSB10), oligonucleotide conjugated antibodies (Ab-oligo) + IS (26, 27, 29)(MITF, TYR, MLANA, CD45) or in the last round, directly conjugated fluorescent antibodies (CD74, HTR2B, GP100, CD25 and CD203c).(9) Fluorescent signal removal between rounds was performed by exposing slides to ultraviolet (UV) light for 15 min. All tissues were counterstained with DAPI, and coverslips were applied with Fluoromount-G mounting media (Invitrogen, Carlsbad, CA). Stained tissues were scanned on the ZEISS AxioScan.Z1 (ZEISS, Germany) with a Colibri 7 light source (ZEISS, Germany). The exposure time was set based upon staining controls. Serial tissue sections were subjected to standard hematoxylin and eosin staining, and brightfield images acquired using the ZEISS AxioScan.Z1 and prepared using image acquisition software ZenBlue (ZEISS, Germany).

## Hybrid cell identification and phenotype analysis in cyclic immunofluorescence images

Images from each round of cyCIF staining were registered and visualized using QiTissue (Quantitative Imaging Systems, Pittsburgh PA). Histogram visualization settings were established for each individual biomarker using negative control serial tissue sections and PBMC slides subjected to the same staining

procedures without antibodies. Cells were segmented in QiTissue using DAPI. After segmentation of all cells within the image, hybrid cells were identified by manual threshold gating of cells based on high mean fluorescent intensity of CD45 combined with each individual tumor marker (MITF+, TYR+, MLANA+, GP100+, HTR2B+). Cells positive for CD45, HTR2B and CD25 or CD203c were not included as they could not be distinguished from basophil or t-regulatory cell populations. Tumor cells were identified by manual threshold gating of cells based on high mean fluorescent intensity of MITF, TYR, MLANA, GP100 and HTR2B (without CD45, CD25 or CD203c). Representative images of hybrid cells from one class 1 and one class 2 patient were included to show heterogeneity in melanocytic tumor marker expression across patient samples and disease stage (Fig. 1). In addition, representative images of TMSB10, GPX1 and CD74 staining in UM tumor sections and in hybrids from peripheral blood were included (Fig. 4). After cyCIF staining, H&E staining was performed and whole globe images were obtained to show localization of hybrid cells within each tumor (Fig. 1).

To determine the percent of hybrid cells and tumor cells expressing CD74, TMSB10, and GPX1, histogram visualization settings were set based on negative staining controls and the minimum intensity value was recorded for each biomarker. A positive cell was identified as a cell having a cell intensity average value of CD74, TMSB10, and GPX1 equal to or greater than the minimum intensity value from QiTissue histogram settings. The percent of biomarker positive hybrid cells and tumor cells were then calculated by dividing the number of positive cells by the total count of hybrid cells or tumor cells then multiplying by 100. The number of percent positive cells were graphed using GraphPad Prism (Boston, MA) and statistical analysis was performed for hybrid cells vs tumor cells using a Welch's t-test where p values > 0.05 were considered statistically significant. Cell intensity average values for each biomarker are reported for all identified hybrid cells and tumor cells within each patient-matched tumor and peripheral blood sample (n = 4 patients, 8 samples) (Supplemental Fig. 7).

## Hybrid cell identification in UM scRNA-seq dataset

The scRNA-seq data downloaded from GEO was processed by following standard procedures as provided in the Seurat package (Version 4.3.0).(30) Briefly, the downloaded filtered count matrix along with barcodes and features were loaded using the Read10X function in Seurat and then was processed through the CreateSeuratObject function with min.cell = 3, resulting in a Seurat object. The loaded Seurat object underwent preprocessing with the SCTransform function using default parameters. It was then subjected to PCA, neighborhood graph construction, cell clustering analysis employing the Leiden algorithm, and dimension reduction via UMAP was performed using functions provided in Seurat. Additionally, heatmap with hierarchical clustering was created using the ComplexHeatmap R package (Version 2.14.0)(31) using the first 50 principal components. For the construction of the neighborhood graph, principal components were selected to account for a cumulative variance of > 95%, while retaining individual variances  $\geq$  5%. For UMAP, the Euclidean distance was used.

To identify clusters potentially containing hybrid cells, the FindMarkers function was first utilized for two cell types based on the annotations provided by the original authors(13) macrophages/monocytes and tumors (encompassing all types of tumor cells, such as Class 1 or Class 2, and Prame+ or Prame- tumor

cells). Subsequently, the AddModuleScore function was invoked twice with nbin = 24 for all samples except UMM063, which used nbin = 12. First, utilizing the top 50 genes that exhibited the highest differential expression scores in tumor cells from FindMarkers, denoted as 'Tum\_Score'. Second, using another set of top 50 genes showing the highest differential expression scores in macrophages/monocytes, referred to as 'Mac\_Score'. These scores were then used to generate violin plots through the VlnPlot function, which were used for the manual identification of hybrid clusters for individual samples.

To identify the doublets and distinguish them from hybrid cells, three simulation-based algorithms were executed: 1.) doubletFinder\_v3 in the DoubletFinder package (Version 2.0.3)(32) with the following parameters, PCs = 1:10, pN = 0.25, pK = 0.09, nExp = 4494, reuse.pANN = FALSE, sct = TRUE); 2.) computeDoubletDensity from scDbtFinder (Version 1.12.0)(33), and 3.) Scrublet (34), which was implemented in a Python package. To run Scrublet in Python, the raw count matrix for each sample was dumped into a CSV file and then loaded into a Python script. For the execution of Scrublet in Python, the raw count matrix for each sample was exported to a CSV file from the Seurat object and then imported into a Python script. The Scrublet results were subsequently exported to CSV files and re-imported into Seurat objects for further analysis and visualization. A cluster-based algorithm implemented as the findDoubletClusters function in scDbtFinder(33), was also employed to identify doublets that may result from fusion of cells from two clusters. However, we believe the results from this algorithm may not align with the goal of this project, which focuses on identifying hybrid cells that can arise from the fusion of two distinct cell types (e.g. macrophages and tumor cells). Therefore, the results produced by this algorithm were not presented.

## Hybrid cell differential gene expression and pathway utilization analysis

Differential gene expression analysis was performed using the FindMarkers function in Seurat for each identified hybrid cell cluster compared to tumor cells and to macrophages for each individual patient. The tumor cells and macrophage cells were selected based on the original cell type annotation(13) after filtering out cells in the identified hybrid clusters. Differentially expressed genes were then annotated using Gene Ontology biological process and molecular function terms (35), cancer gene consortium tier and cancer hallmarks from COSMIC database(36) and through manual literature review. Genes were selected for visualization in Fig. 3 based on the following criteria: statistical significance according to adjusted p-value  $\leq 0.05$ , log<sub>2</sub> fold change  $\geq 1.0$  for upregulated genes or  $\leq -1.0$  for downregulated genes, and present in at least two patient samples. For some comparisons (hybrid vs tumor up-regulated genes and hybrid vs macrophage down-regulated genes) this filtering method resulted in too many genes for visualization. Therefore, the lists were further narrowed down by first ranking genes according to adjusted p-value and then selecting the top 10 genes for hybrid vs tumor upregulated, or only including genes with a log<sub>2</sub> fold change  $\leq -2.0$  for hybrid vs macrophage downregulated. Genes that were significantly differentially expressed in all patient samples and were annotated to be involved in the hallmarks of cancer according to the cancer hallmarks gene database were also included. Furthermore, significant



genes that were present in all four class 2 tumor hybrids and were involved in top pathways from our pathway analysis (described below) were also included. This expanded our gene list to include the following additional genes: *GPX1*, *SEPP1*, *B2M*, *RHOA*, *CD68*, *CD14*, *TMSB10*, *TYROBP*, *ACTB*, and *S100A11*. In total, 50 genes were selected for visualization.

For pathway analysis, all differentially expressed genes for hybrid vs tumor clusters and hybrid vs macrophage clusters were selected from each individual patient based on the following criteria: an adjusted p value  $\leq 0.05$  and a log2 fold change  $\geq 0.58$  or  $\leq -0.58$ . Pathway enrichment analysis was performed individually for each patient using the Reactome analysis RESTful API. (37)

## Ligand-receptor interaction

The Python package, CellphoneDB (Version 4.0.0) (38), was used to investigate ligand-receptor interactions among annotated cell types and identified hybrid cell cluster for individual patients. To this end, the raw counts were loaded as AnnData objects using Scanpy (Version 1.9.0) after being exported in the h5ad format from the Seurat object in R. The statistical inference of interaction specificity method was utilized with default parameters, including 1,000 iterations, p value threshold of 0.05, and subsampling set to False. The CellphoneDB results were visualized using another Python package, ktplotsy (Version 0.1.10, <https://github.com/zktuong/ktplotsy>) and exported into CSV files for further analysis. To create Fig. 4B, only four cell types were chosen, ensuring that each cell type appeared in all patients and has a minimum of 20 cells in each sample. The entire workflow was developed as a Python script, CellPhoneDBNotebook.py, along with a Jupyter notebook, CellPhoneDBNotebook.ipynb, both of which have been released on [https://github.com/AshleyNAnderson/UVM\\_scRNA\\_Hybrid\\_Manuscript](https://github.com/AshleyNAnderson/UVM_scRNA_Hybrid_Manuscript).

## Code availability

The workflow to identify hybrid clusters for individual patients was implemented in R (Version 4.2.3) except the Scrublet doublet identification, which was implemented in Python. The ligand-receptor interaction inference was implemented in Python (Version 3.10). All code is available at

[https://github.com/AshleyNAnderson/UVM\\_scRNA\\_Hybrid\\_Manuscript](https://github.com/AshleyNAnderson/UVM_scRNA_Hybrid_Manuscript) .

## Results

Identification of tumor-immune hybrid cells in UM primary tumors using multiplexed cyCIF. We previously published that CHCs are detected at higher levels than CTCs in peripheral blood of patients with UM. Moreover, higher levels of CHCs were predictive of poor overall survival, whereas CTCs were not predictive.(9) To determine if neoplastic-immune hybrid cells were present in primary tumors, we first analyzed primary UM FFPE sections using multiplexed cyCIF. We identified UM-associated hybrid cells based on co-expression of melanocytic tumor proteins: Microphthalmia-associated transcription factor (MITF), Tyrosinase (TYR), Melan-A (MLANA), premelanosome protein (PMEL, GP100), 5-hydroxytryptamine receptor 2B (HTR2B) and the pan-leukocyte marker CD45 (Fig. 1). As HTR2B and CD45 are also expressed on basophils and T-regulatory cells, CD25 and CD203c were used to exclude

these immune populations. Hybrid cells (CD45 co-expressed with one or more melanocyte markers) were identified in both class 1 (Fig. 1A; n = 1) and class 2 (Fig. 1B; n = 3) UM tissue sections. Of note, UM-associated hybrids harbored heterogeneous expression patterns of UM-specific proteins, similar to our reported findings of UM-derived CHCs where class 2 hybrids commonly expressed HTR2B compared to class 1 hybrids. (9)

Identification of tumor-immune hybrid cells in UM primary tumors using scRNA sequencing. Analysis of a single tissue section from a FFPE tumor block represents only a small fraction of the resected tumor. Given the relative rarity of hybrid cells compared to other cell types within a tumor, we sought to more comprehensively identify and phenotype hybrid cells within UM tumors by leveraging a previously published single cell RNA sequencing (scRNA-seq) UM dataset. (13) Using both a Leiden community detection algorithm (39) (Fig. 2A) and a hierarchical clustering method (31) (**Supplemental Fig. 1**) we clustered cells from each individual patient sample and annotated cell clusters based on the original gene cell identity markers provided by Durante et al. (13) In five out of eight primary tumor samples, we identified one or more clusters of hybrid cells (Fig. 2B and **Supplemental Files 2–5**) based on co-expression of tumor genes *MITF*, *MLANA*, *DCT*, *TYR*, *GP100*, and *HTR2B*, and macrophage genes *CD45*, *CD14*, *CD163* (Fig. 2C-2E for patient UMM059. See Supplemental Figs. 2–5 for other four patients). To determine the extent of discrete lineage co-expression in identified tumor-macrophage hybrid cells, we generated a composite tumor gene expression score and a macrophage gene expression score using the top 50 marker genes identified by differential gene expression analysis between cells annotated as tumors and cells annotated as macrophage/monocytes. We then ranked each cell cluster by their respective tumor score and macrophage score. We determined that hybrid cell clusters expressed tumor genes at significantly higher levels than immune cell clusters (Fig. 2F, patient UMM059, all cluster comparisons  $p \leq 2 \times 10^{-08}$  and all other patients in **Supplemental Figs. 2–5**), and that hybrid clusters showed significantly higher macrophage gene expression scores than all other tumor clusters (Fig. 2G, all cluster comparisons  $p \leq 2 \times 10^{-16}$ ). For patient samples UMM059, UMM064, UMM065, and UMM066, only one hybrid cell cluster was identified, and contained a range of 191–501 hybrid cells (**Supplemental Table 2**). In patient sample UMM063, two hybrid cell clusters were identified, and differential gene expression analysis between these two hybrid clusters revealed one cluster (i.e., cluster 3) with a greater inflammatory gene expression profile than the second hybrid cluster (i.e., cluster 12), which was characterized by high expression of *IL1B*, *NFKBIA*, *CCL3*, *CXCL1-3* and *TNF* genes. (Complete list of differentially expressed genes and pathways in **Supplemental File 1**).

Hybrid cells are a distinct subpopulation from sequencing artifact doublets. One consequence of droplet-based scRNA-seq methods is the potential for sequencing doublets, or artifactual libraries generated from two or more cells that adhered together during sample preparation. To confirm that identified hybrid cells are distinct single cells and not macrophage and tumor cell doublets, we performed rigorous doublet detection using three simulation-based methods: Scrublet (34), DoubletFinder (32), and computeDoubletDensity from scDblFinder. (33) We found that for all three methods hybrid cell clusters did not have consistently elevated doublet scores compared to the majority of clusters across all patient

samples (**Supplemental Fig. 6**). These results indicate that hybrids cells represent a distinct cluster of single cells rather than a cluster of artifactual sequencing doublets of tumor cells and immune cells produced during the sample preparation.

Differential gene expression and pathway utilization of tumor-immune hybrids. After identifying hybrid cell clusters, we evaluated differences in gene expression and pathway enrichment among hybrid cells compared to non-hybrid tumor cells and macrophage cell populations. Differential gene expression analysis was performed independently for each patient sample (**Supplemental File 2**). We focused our evaluation on differentially expressed genes that were significantly upregulated or downregulated (adjusted p value  $\leq 0.05$  and log2 fold change  $\geq 1.0$  or  $\leq -1.0$ ) and were shared in at least two patient samples (Fig. 3A, B). Gene function was evaluated by annotation through the Gene Ontology database, annotation in the COSMIC cancer gene census database, by manual curation guided by literature review, and through pathway enrichment analysis using Reactome. (37) Our results identified critical features of metastasis and tumor progression in hybrid cells, including genes and pathways involved in cell migration and invasion (*TMSB10*, *AIF1*, *ARGHDIB*, *CAPG*, *RHOA*, *TYROBP*, *ACTB*, *S100A11*), immune evasion (*CD74*, *B2M*, *TNFAIP3*), and altered metabolism (*GPX1*, *SEPP1*, *UQCRB*) (Fig. 3C and **Supplemental File 3**). These observations support a role for hybrid cells in UM metastatic progression.

Hybrid cell phenotypes within patient-matched primary tumor and peripheral blood. We sought to verify hybrid cell expression of proteins from each identified pathway: cell motility, immune evasion, and metabolism. The markers TMSB10, CD74 and GPX1 were chosen based on their upregulated expression across all patient samples in the single cell RNA sequencing dataset. Using patient matched FFPE tumor sections and peripheral blood mononuclear cell (PBMC) slides, we applied our panel of melanocytic (MITF, TYR, MLANA, GP100, and HTR2B) and immune antibodies (CD45, CD25, CD203c) as described in Fig. 1 to identify hybrid cell populations in addition to antibodies for TMSB10, CD74 and GPX1. After identifying all hybrid cells within a tissue section or peripheral blood slide (Fig. 4A and 4B), we quantified the average fluorescent intensity of each phenotypic marker TMSB10, CD74 and GPX1 across all hybrid and tumor cells from each patient (**Supplemental Fig. 7**). We show that the number of percent positive cells for both hybrid and tumor cells within primary tumors were similar for all three markers (Fig. 4C, all hybrids vs non-hybrids in tumor not significant p value  $\geq 0.05$ ). However, within peripheral blood, we show that hybrid cells have a significantly higher number of cells positive for TMSB10 and GPX1 (Fig. 4C, TMSB10 p value = 0.03 and GPX1 p value = 0.04) than CTCs. Although CD74 was not found to be significantly higher in hybrid cells than CTCs (p value = 0.76), a higher number of hybrid cells were positive for CD74 in the peripheral blood than in the primary tumor-resident hybrids (p value = 0.03). In addition, more disseminated hybrid cells expressed GPX1 than tumor-resident hybrids (p value = 0.007). These findings suggest that TMSB10, GPX1 and CD74 play an important role in successful hybrid cell dissemination and/or survival in circulation.

Hybrid cell ligand-receptor signaling within the primary tumor. To understand how hybrid cells may interact with or influence other cells in the tumor microenvironment we predicted ligand-receptor cell-cell interactions between hybrid cells and other cells within the tumor using cellPhoneDB.(38) Across all five

patient samples, we determined that the identified hybrid clusters displayed far fewer inferred significant interactions with other cell types (Fig. 5A), suggesting that hybrid cells may be less dependent on other cells to maintain their functional behavior and thus may be more prone to metastasis.(40) We also identified a conserved interaction between tyrosinase binding protein (TYROBP) present on hybrid cells and CD44 present on tumor cells, in all patients (Fig. 5B and **Supplemental File 4**) (41, 42). Although little is known regarding TYROBP-CD44 signaling in cancer, *TYROBP* has been previously shown as highly expressed in clear cell renal cell carcinoma CTCs. (42) Furthermore, we identified a conserved interaction between Amyloid beta precursor protein (APP) on macrophages and tumor cells, signaling to CD74 present on hybrid cells, as well as annexin A1 (ANXA1) – formyl peptide receptor 1 (FPR1) and ANXA1-FPR3 signaling between hybrids and macrophages in four of five patients. APP-CD74 signaling has been previously implicated in uveal melanoma (43), where high expression of APP was identified in UM primary tumors compared to lower APP and higher CD74 expression in metastatic UM tumors. In addition, ANXA1-FPR1 and ANXA1-FPR3 signaling have been shown to increase the invasiveness and survival of breast cancer and colorectal cancer cells. (44–46) Other signaling pathways with established roles in promoting cancer metastasis were also significantly expressed in hybrid cell populations including GAS6-AXL (19) (tumor-hybrid), CXCL12-CXCR4 (20) (hybrid- T cells), LGALS9-P4HB (21) (hybrid-tumor), and IGF1-IGF1R (22–25) (hybrid-tumor). Collectively, these signaling pathways in hybrid cell populations suggest that hybrid cells retain key cell-cell communication between tumor and immune cells with established roles in promoting metastasis including actin remodeling, angiogenesis, EMT, and UM metastatic seeding of the liver via IGF1-IGF1R signaling.

## Discussion

The evaluation of distinct subsets of tumor cell types involved in dissemination and seeding of metastatic sites is pivotal for uncovering key mechanisms underlying cancer metastasis and for subsequent development of targeted therapeutic strategies. In this study we investigated the role of the predominant circulating neoplastic cell type in uveal melanoma, neoplastic-immune hybrid cells, by examining their discrete features within primary uveal melanoma tumors before they disseminate. Herein, we applied multiplexed cyCIF and analyzed a scRNA-seq dataset to identify and uncover key features of UM-derived hybrid cells. Using bioinformatic approaches to identify a subpopulation of melanoma cells that harbor immune cell gene expression, we determined that tumor-immune hybrid cells within the primary UM scRNA-seq dataset predominantly expressed macrophage-specific genes. Analyses of hybrid cell gene expression profiles relative to non-hybrid UM cells revealed pathway enrichment and ligand-receptor cell signaling that are involved in governing metastasis. Specifically, we found that hybrid cells retain signaling pathways common to tumor cells and macrophages that have been previously implicated in mediating one or more aspects of the hallmarks of cancer metastasis including TYROBP-CD44, APP-CD74, ANXA1-FPR1/3, GAS6-AXL, CXCL12-CXCR4, LGALS9-P4HB, and IGF1-IGFR1 and that these pathways were conserved in at least two or more patient samples. Furthermore, we verified that hybrid cells within the primary tumor and in peripheral blood express TMSB10, CD74 and GPX1 at the protein level, and that TMSB10 and GPX1 are significantly upregulated in disseminated hybrid cells

compared to CTCs. These insights shed light on the significance of hybrid cells within the tumor microenvironment and highlight potential mechanisms that impact their disease spread.

The upregulation of genes and pathways that confer migratory properties observed in UM hybrid cells suggest their active involvement in metastasis. This includes the upregulated expression of genes associated with actin dynamics and cell motility, *TMSB10*, *AIF1*, *ARGHDIB*, *CAPG*, *RHOA*, *TYROBP*, *ACTB*, and *S100A11*, and supports the notion that UM hybrid cells are endowed with a migratory phenotype that facilitates their invasion and enhanced dissemination into peripheral blood. (41, 42, 47–55) In addition, we also found that *TMSB10* was upregulated in CHCs compared to CTCs at the protein level. These findings are consistent with our prior reports of hybrid cells in colorectal cancer and cutaneous melanoma (7) which demonstrate that *in vitro*-derived hybrid cells, derived from fusion between tumor and immune cells, display increased migratory phenotypes and respond to macrophage chemotaxis. Hybrid cell expression of cell signaling pathways that mediate actin remodeling, cell migration and EMT, specifically *GAS6-AXL* (tumor-hybrid) and *LGALS9-P4HB* (hybrid-tumor), also align with increased migratory phenotypes of hybrid cells. (19, 21) Hybrid cell expression of many genes and pathways involved in regulating cell migration aligns with the metastatic cascade and emphasizes the potential of UM hybrid cells as an early indicator of increased metastatic potential.

Hybrid cell expression of immune evasion pathways highlights their potential role in escaping immune surveillance, a hallmark of cancer progression. Our results reveal hybrid cell upregulation of immune molecules, including *CD74*, *B2M* and *TNFAIP3*, which are known to contribute to cancer cell immune evasion. (56–59) Although *CD74* expression was not significantly higher in hybrid cells than tumor cells at the protein level, it was highly enriched in cells within circulation compared to those within the primary tumor. This indicates that UM hybrid cells may have a selective advantage in avoiding immune detection, allowing them to escape from the primary tumor microenvironment and traverse the bloodstream without being targeted by immune effector cells. This phenomenon could contribute to their successful dissemination and eventual establishment of metastatic foci. (60)

Our findings also highlight alterations in cell metabolism in UM hybrid cells, which could confer a survival advantage during their journey across the metastatic cascade. Hybrid cell upregulation of Reactome pathways “metabolism of proteins” and “iron uptake and transport” point to a metabolic shift that may enable hybrid cells to survive within the primary tumor microenvironment and survive the challenging conditions encountered during circulation. (61, 62) This metabolic reprogramming could be instrumental in promoting their survival and subsequent metastatic colonization within the liver. In addition, hybrid cells displayed upregulated expression of ubiquinol-cytochrome c reductase binding protein (*UQCRB*), which has been shown to promote angiogenesis and cancer cell survival, that may facilitate hybrid cell dissemination into peripheral blood. (63, 64) We also found that UM hybrid cells displayed upregulated expression of metabolic genes commonly expressed within the liver including *GPX1* and *SEPP1*, as well as IGF1-IGFR1 signaling where IGF1 is primarily produced by the liver. Within peripheral blood, *GPX1* expression at the protein level was significantly higher in hybrid cells than CTCs. Increased expression of these proteins and signaling pathways within hybrid cells may contribute to the selective metastatic

seeding of UM to the liver and highlight an important organotrophic mechanism of UM metastasis that should be validated further in future studies. (65, 66)

The converging pathways of immune evasion, enhanced migration, and altered metabolism shared across UM hybrid cells highlight their potential as key players in the metastatic process. While the exact mechanisms linking these features remain to be elucidated, their interplay likely orchestrates a synergistic effect of the combined tumor and immune cell biology that confers a survival advantage to UM hybrid cells within the unfamiliar environment of the circulatory system and selective seeding within the liver metastatic site.

The implications of our findings extend to both clinical and therapeutic realms. The identification of UM hybrid cells in circulation as a non-invasive biomarker offers a promising avenue for non-invasive prognostication and early detection of metastasis. This allows for timely intervention without the need for invasive biopsy procedures which carry risk to patients, may not detect tumor heterogeneity, and are not repeatable. Studies examining the mechanisms of hybrid cell dissemination will improve the clinical utility as a circulating biomarker. Furthermore, targeting the unique characteristics of UM hybrid cells, such as their upregulated genes *GPX1* or *SEPP1*, could pave the way for the development of novel therapeutic strategies aimed at disrupting the metastatic process in UM.

It is important to note that this work is limited by a small tumor sample size, as well as the limited number of sequenced cells from some biopsies. Large datasets of UM scRNA-seq do not yet exist, thus this work should be further validated in larger cohorts in the future. In addition, this study focuses primarily on tumor-macrophage hybrid cells, however other tumor-immune hybrid cell types were identified in this dataset including tumor-T cell hybrids (results not shown), albeit at much smaller numbers. Further investigations are warranted to explore the mechanistic effects of these findings in models of UM metastasis, in particular the organotrophic effects of *GPX1*, *SEPP1* and IGF1-IGF1R signaling in disseminated hybrid cells.

## Conclusions

In conclusion, our study highlights an exciting role for hybrid cells in unraveling the complexities of UM metastasis. Hybrid cell expression of immune evasion pathways, enhanced migratory properties, and altered cell metabolism shared across patients and disease stages provides insights into the mechanisms driving successful dissemination, survival in circulation, and eventual establishment of metastatic lesions.

## Abbreviations

UM, uveal melanoma; CHCs, circulating hybrid cells; CTCs, circulating tumor cells; cyCIF, cyclic immunofluorescence, scRNA-seq, single cell RNA sequencing; SEPP1, selenoprotein p; GPX1, glutathione peroxidase; TMSB10, thymosin beta 10; GAS6, growth arrest specific 6; AXL, AXL receptor tyrosine kinase;

CXCL12, C-X-C motif chemokine ligand 12; CXCR4, C-X-C motif chemokine receptor 4; LGALS9, galectin 9; P4HB, propel 4-hydroxylase subunit beta; IGF1, insulin-like growth factor 1; IGF1R, insulin-like growth factor 1 receptor; EMT, epithelial to mesenchymal transition; FFPE, formalin fixed paraffin embedded; PBMCs, peripheral blood mononuclear cells; PFA, paraformaldehyde; PBS, phosphate buffered saline; SSC, saline sodium citrate; IS, imaging strands; Ab-oligo, oligonucleotide conjugated antibody; UV, ultraviolet; MITF, microphthalmia-associated transcription factor; TYR, tyrosinase; MLANA, melan-A; PMEL/GP100 (premelanosome protein); HTR2B, 5-hydroxytryptamine receptor 2B; TYROBP, tyrosinase binding protein; APP amyloid beta precursor protein; ANXA1, annexin A1; FPR1, formyl peptide receptor;

## **Declarations**

### **Ethics Approval and Consent to Participate**

All human formalin-fixed paraffin-embedded (FFPE) tissue samples and peripheral blood specimens were collected and analyzed in accordance with ethical requirements and regulations of the Oregon Health and Science University institutional review board. Informed consent was obtained from all subjects and studies were conducted under approved IRB protocol (IRB0005169).

### **Consent for Publication**

Not applicable

### **Availability of data and materials**

For scRNA-seq analyses all code is available at

[https://github.com/AshleyNAnderson/UVM\\_scRNA\\_Hybrid\\_Manuscript](https://github.com/AshleyNAnderson/UVM_scRNA_Hybrid_Manuscript). Sequencing data from this study was downloaded from the GEO entry GSE139829, available at

<https://www.ncbi.nlm.nih.gov/geo/query/acc.cgi?acc=GSE139829>.

The RAW data file (<https://www.ncbi.nlm.nih.gov/geo/download/?acc=GSE139829&format=file>) was utilized. The meta data for individual cells, including cell barcodes and annotated cell types, were directly provided by the original authors.(13) For cyCIF studies, all RAW imaging files are available from the corresponding author upon reasonable request. All other data generated and analyzed during this study are included in this published article [and its supplementary information files].

### **Competing Interests**

A.H.S. is a Consultant for Castle Biosciences, Inc.

### **Funding**

This research was supported by the National Institutes of Health (Bethesda, MD) P30 EY010572 core grant (A.H.S.), the Malcolm M. Marquis, MD Endowed Fund for Innovation (A.H.S.), an unrestricted grant from Research to Prevent Blindness (New York, NY) to Casey Eye Institute, Oregon Health & Science University (A.H.S.), the American Association for Cancer Research Ocular Melanoma Foundation (A.H.S.), Melanoma Research Foundation (A.H.S.), Medical Research Foundation (A.H.S.), National Human Genome Research Institute, 5U41HG003751 and U24HG012198 (G.W.); National Cancer Institute, 5U01CA239069 (G.W.), National Library of Medicine, 5T15LM007088 (C.D.K.), National Institutes of Health/National Cancer Institute, P30CA069533 (M.H.W.), National Institutes of Health/National Cancer Institute, R44CA250861 (M.H.W., S.L.G.), Melanoma Research Foundation Medical Student Award (A.N.A.), National Institutes of Health/National Institute of General Medical Sciences, T32GM141938 (A.N.A.) and National Cancer Institute F31CA271676 (A.N.A.).

## Author Contributions

Conceptualization, A.N.A., S.K.S., A.H.S., G.W., M.H.W.; methodology, A.N.A., P.C., C.D.K., S.K.S., A.P., H.C.F., A.R.G., A.D.D., J.A.J., S.L.G., M.H.W.; formal analysis, A.N.A., P.C., C.D.K., G.W., M.H.W.; data curation, A.N.A., P.C., C.D.K., A.P., H.C.F., A.R.G., A.D.D., G.W.; writing—original draft preparation, A.N.A., G.W., M.H.W.; writing—reviewing and editing, A.N.A., C.D.K., S.K.S., A.P., H.C.F., A.R.G., A.D.D., Y.F., J.A.J., S.L.G., A.H.S., G.W., M.H.W.; resources, A.H.S., S.L.G., G.W., M.H.W.; supervision and project administration, A.H.S., S.L.G., G.W., M.H.W.; funding acquisition, A.N.A., C.D.K., A.H.S., G.W., M.H.W.; All authors have read and agreed to the published version of the manuscript.

## Acknowledgements

We would like to thank the Advanced Light Microscopy Core at Oregon Health and Science University, Drs. William Harbour and Michael Durante for their collaboration in using their scRNA-sequencing dataset, Dr. Andrew Adey for scientific advice on doublet detection methods, Noah Mozell, Megan Lonhart, Nicole Giske and Trinity Robinson for technical assistance with antibody validation, differential gene expression and pathway enrichment analyses, and Dr. Young Hwan Chang and Zachary Sims for assistance with multiplex image registration for the cyCIF studies.

## References

1. Carvajal RD, Schwartz GK, Tezel T, Marr B, Francis JH, Nathan PD. Metastatic disease from uveal melanoma: treatment options and future prospects. *Br J Ophthalmol*. 2017;101(1):38-44.
2. Kuk D, Shoushtari AN, Barker CA, Panageas KS, Munhoz RR, Momtaz P, et al. Prognosis of Mucosal, Uveal, Acral, Nonacral Cutaneous, and Unknown Primary Melanoma From the Time of First Metastasis. *Oncologist*. 2016;21(7):848-54.
3. Krantz BA, Dave N, Komatsubara KM, Marr BP, Carvajal RD. Uveal melanoma: epidemiology, etiology, and treatment of primary disease. *Clin Ophthalmol*. 2017;11:279-89.



4. Jager MJ, Shields CL, Cebulla CM, Abdel-Rahman MH, Grossniklaus HE, Stern MH, et al. Uveal melanoma. *Nat Rev Dis Primers*. 2020;6(1):24.
5. Onken MD, Worley LA, Char DH, Augsburger JJ, Correa ZM, Nudleman E, et al. Collaborative Ocular Oncology Group report number 1: prospective validation of a multi-gene prognostic assay in uveal melanoma. *Ophthalmology*. 2012;119(8):1596-603.
6. Chattopadhyay C, Kim DW, Gombos DS, Oba J, Qin Y, Williams MD, et al. Uveal melanoma: From diagnosis to treatment and the science in between. *Cancer*. 2016;122(15):2299-312.
7. Gast CE, Silk AD, Zarour L, Riegler L, Burkhart JG, Gustafson KT, et al. Cell fusion potentiates tumor heterogeneity and reveals circulating hybrid cells that correlate with stage and survival. *Sci Adv*. 2018;4(9):eaat7828.
8. Dietz MS, Sutton TL, Walker BS, Gast CE, Zarour L, Sengupta SK, et al. Relevance of circulating hybrid cells as a non-invasive biomarker for myriad solid tumors. *Scientific Reports*. 2021;11(1).
9. Parappilly MS, Chin Y, Whalen RM, Anderson AN, Robinson TS, Strgar L, et al. Circulating Neoplastic-Immune Hybrid Cells Predict Metastatic Progression in Uveal Melanoma. *Cancers (Basel)*. 2022;14(19).
10. Roh-Johnson M, Shah AN, Stonick JA, Poudel KR, Kargl J, Yang GH, et al. Macrophage-Dependent Cytoplasmic Transfer during Melanoma Invasion In Vivo. *Dev Cell*. 2017;43(5):549-62.e6.
11. Manjunath Y, Porciani D, Mitchem JB, Suvilesh KN, Avella DM, Kimchi ET, et al. Tumor-Cell-Macrophage Fusion Cells as Liquid Biomarkers and Tumor Enhancers in Cancer. *Int J Mol Sci*. 2020;21(5).
12. Manjunath Y, Porciani D, Mitchem JB, Suvilesh KN, Avella DM, Kimchi ET, et al. Tumor-Cell-Macrophage Fusion Cells as Liquid Biomarkers and Tumor Enhancers in Cancer. *International Journal of Molecular Sciences*. 2020;21(5):1872.
13. Durante MA, Rodriguez DA, Kurtenbach S, Kuznetsov JN, Sanchez MI, Decatur CL, et al. Single-cell analysis reveals new evolutionary complexity in uveal melanoma. *Nature Communications*. 2020;11(1).
14. Gerstberger S, Jiang Q, Ganesh K. Metastasis. *Cell*. 2023;186(8):1564-79.
15. Davis RT, Blake K, Ma D, Gabra MBI, Hernandez GA, Phung AT, et al. Transcriptional diversity and bioenergetic shift in human breast cancer metastasis revealed by single-cell RNA sequencing. *Nat Cell Biol*. 2020;22(3):310-20.
16. Park HA, Brown SR, Kim Y. Cellular Mechanisms of Circulating Tumor Cells During Breast Cancer Metastasis. *Int J Mol Sci*. 2020;21(14).
17. Zhao Y, Wang H, Zhou J, Shao Q. Glutathione Peroxidase GPX1 and Its Dichotomous Roles in Cancer. *Cancers (Basel)*. 2022;14(10).
18. Barrett CW, Reddy VK, Short SP, Motley AK, Lintel MK, Bradley AM, et al. Selenoprotein P influences colitis-induced tumorigenesis by mediating stemness and oxidative damage. *J Clin Invest*. 2015;125(7):2646-60.

19. Zdzalik-Bielecka D, Poświata A, Kozik K, Jastrzębski K, Schink KO, Brewińska-Olchowik M, et al. The GAS6-AXL signaling pathway triggers actin remodeling that drives membrane ruffling, macropinocytosis, and cancer-cell invasion. *Proc Natl Acad Sci U S A*. 2021;118(28).
20. Guo F, Wang Y, Liu J, Mok SC, Xue F, Zhang W. CXCL12/CXCR4: a symbiotic bridge linking cancer cells and their stromal neighbors in oncogenic communication networks. *Oncogene*. 2016;35(7):816-26.
21. Ma X, Wang J, Zhuang J, Ma X, Zheng N, Song Y, et al. P4HB modulates epithelial-mesenchymal transition and the  $\beta$ -catenin/Snail pathway influencing chemoresistance in liver cancer cells. *Oncol Lett*. 2020;20(1):257-65.
22. Xu L, Zhou R, Yuan L, Wang S, Li X, Ma H, et al. IGF1/IGF1R/STAT3 signaling-inducible IFITM2 promotes gastric cancer growth and metastasis. *Cancer Lett*. 2017;393:76-85.
23. Yoshida M, Selvan S, McCue PA, DeAngelis T, Baserga R, Fujii A, et al. Expression of insulin-like growth factor-1 receptor in metastatic uveal melanoma and implications for potential autocrine and paracrine tumor cell growth. *Pigment Cell Melanoma Res*. 2014;27(2):297-308.
24. Wang X, Zhu Q, Lin Y, Wu L, Wu X, Wang K, et al. Crosstalk between TEMs and endothelial cells modulates angiogenesis and metastasis via IGF1-IGF1R signalling in epithelial ovarian cancer. *Br J Cancer*. 2017;117(9):1371-82.
25. Hirakawa T, Yashiro M, Doi Y, Kinoshita H, Morisaki T, Fukuoka T, et al. Pancreatic Fibroblasts Stimulate the Motility of Pancreatic Cancer Cells through IGF1/IGF1R Signaling under Hypoxia. *PLoS One*. 2016;11(8):e0159912.
26. McMahon NP, Jones JA, Kwon S, Chin K, Nederlof MA, Gray JW, et al. Oligonucleotide conjugated antibodies permit highly multiplexed immunofluorescence for future use in clinical histopathology. *J Biomed Opt*. 2020;25(5):1-18.
27. McMahon NP, Jones JA, Anderson AN, Dietz MS, Wong MH, Gibbs SL. Flexible Cyclic Immunofluorescence (cyCIF) Using Oligonucleotide Barcoded Antibodies. *Cancers (Basel)*. 2023;15(3).
28. McMahon N, Jones J, Eng J, Kwon S, Chang YH, Thibault G, et al. Signal removal methods for highly multiplexed immunofluorescent staining using antibody conjugated oligonucleotides. *Proc SPIE Int Soc Opt Eng*. 2019;10881.
29. Jones JA, McMahon NP, Zheng T, Eng J, Chin K, Kwon S, et al. Oligonucleotide conjugated antibody strategies for cyclic immunostaining. *Sci Rep*. 2021;11(1):23844.
30. Butler A, Hoffman P, Smibert P, Papalexi E, Satija R. Integrating single-cell transcriptomic data across different conditions, technologies, and species. *Nat Biotechnol*. 2018;36(5):411-20.
31. Gu Z, Hübschmann D. Make Interactive Complex Heatmaps in R. *Bioinformatics*. 2022;38(5):1460-2.
32. McGinnis CS, Murrow LM, Gartner ZJ. DoubletFinder: Doublet Detection in Single-Cell RNA Sequencing Data Using Artificial Nearest Neighbors. *Cell Syst*. 2019;8(4):329-37.e4.
33. Germain PL, Lun A, Garcia Meixide C, Macnair W, Robinson MD. Doublet identification in single-cell sequencing data using scDbtFinder. *F1000Res*. 2021;10:979.

34. Wolock SL, Lopez R, Klein AM. Scrublet: Computational Identification of Cell Doublets in Single-Cell Transcriptomic Data. *Cell Syst.* 2019;8(4):281-91.e9.
35. Ashburner M, Ball CA, Blake JA, Botstein D, Butler H, Cherry JM, et al. Gene ontology: tool for the unification of biology. The Gene Ontology Consortium. *Nat Genet.* 2000;25(1):25-9.
36. Tate JG, Bamford S, Jubb HC, Sondka Z, Beare DM, Bindal N, et al. COSMIC: the Catalogue Of Somatic Mutations In Cancer. *Nucleic Acids Res.* 2019;47(D1):D941-d7.
37. Gillespie M, Jassal B, Stephan R, Milacic M, Rothfels K, Senff-Ribeiro A, et al. The reactome pathway knowledgebase 2022. *Nucleic Acids Res.* 2022;50(D1):D687-d92.
38. Efremova M, Vento-Tormo M, Teichmann SA, Vento-Tormo R. CellPhoneDB: inferring cell-cell communication from combined expression of multi-subunit ligand-receptor complexes. *Nat Protoc.* 2020;15(4):1484-506.
39. Traag VA, Waltman L, van Eck NJ. From Louvain to Leiden: guaranteeing well-connected communities. *Sci Rep.* 2019;9(1):5233.
40. Ye X, Huang X, Fu X, Zhang X, Lin R, Zhang W, et al. Myeloid-like tumor hybrid cells in bone marrow promote progression of prostate cancer bone metastasis. *J Hematol Oncol.* 2023;16(1):46.
41. Lu J, Peng Y, Huang R, Feng Z, Fan Y, Wang H, et al. Elevated TYROBP expression predicts poor prognosis and high tumor immune infiltration in patients with low-grade glioma. *BMC Cancer.* 2021;21(1):723.
42. Guo L, An T, Zhou H, Wan Z, Huang Z, Chong T. MMP9 and TYROBP affect the survival of circulating tumor cells in clear cell renal cell carcinoma by adapting to tumor immune microenvironment. *Sci Rep.* 2023;13(1):6982.
43. Sun S, Guo B, Xu L, Shi R. Integrated analysis reveals the dysfunction of signaling pathways in uveal melanoma. *BMC Cancer.* 2022;22(1):734.
44. Vecchi L, Alves Pereira Zóia M, Goss Santos T, de Oliveira Beserra A, Colaço Ramos CM, França Matias Colombo B, et al. Inhibition of the AnxA1/FPR1 autocrine axis reduces MDA-MB-231 breast cancer cell growth and aggressiveness in vitro and in vivo. *Biochim Biophys Acta Mol Cell Res.* 2018;1865(9):1368-82.
45. Cheng TY, Wu MS, Lin JT, Lin MT, Shun CT, Huang HY, et al. Annexin A1 is associated with gastric cancer survival and promotes gastric cancer cell invasiveness through the formyl peptide receptor/extracellular signal-regulated kinase/integrin beta-1-binding protein 1 pathway. *Cancer.* 2012;118(23):5757-67.
46. Foo SL, Sachaphibulkij K, Lee CLY, Yap GLR, Cui J, Arumugam T, et al. Breast cancer metastasis to brain results in recruitment and activation of microglia through annexin-A1/formyl peptide receptor signaling. *Breast Cancer Res.* 2022;24(1):25.
47. Zhang X, Ren D, Guo L, Wang L, Wu S, Lin C, et al. Thymosin beta 10 is a key regulator of tumorigenesis and metastasis and a novel serum marker in breast cancer. *Breast Cancer Res.* 2017;19(1):15.

48. Yan Z, Yan Q, Song Y, Wang L. TMSB10, a potential prognosis prediction biomarker, promotes the invasion and angiogenesis of gastric cancer. *J Gastroenterol Hepatol.* 2021;36(11):3102-12.
49. Li Z, Li Y, Tian Y, Li N, Shen L, Zhao Y. Pan-cancer analysis identifies the correlations of Thymosin Beta 10 with predicting prognosis and immunotherapy response. *Front Immunol.* 2023;14:1170539.
50. Li T, Feng Z, Jia S, Wang W, Du Z, Chen N, et al. Daintain/AIF-1 promotes breast cancer cell migration by up-regulated TNF- $\alpha$  via activate p38 MAPK signaling pathway. *Breast Cancer Res Treat.* 2012;131(3):891-8.
51. Glaser J, Neumann MH, Mei Q, Betz B, Seier N, Beyer I, et al. Macrophage capping protein CapG is a putative oncogene involved in migration and invasiveness in ovarian carcinoma. *Biomed Res Int.* 2014;2014:379847.
52. O'Connor K, Chen M. Dynamic functions of RhoA in tumor cell migration and invasion. *Small GTPases.* 2013;4(3):141-7.
53. Liu H, Seynhaeve ALB, Brouwer RWW, van IWFJ, Yang L, Wang Y, et al. CREPT Promotes Melanoma Progression Through Accelerated Proliferation and Enhanced Migration by RhoA-Mediated Actin Filaments and Focal Adhesion Formation. *Cancers (Basel).* 2019;12(1).
54. Suresh R, Diaz RJ. The remodelling of actin composition as a hallmark of cancer. *Transl Oncol.* 2021;14(6):101051.
55. Jaiswal JK, Lauritzen SP, Scheffer L, Sakaguchi M, Bunkenborg J, Simon SM, et al. S100A11 is required for efficient plasma membrane repair and survival of invasive cancer cells. *Nat Commun.* 2014;5:3795.
56. Imaoka M, Tanese K, Masugi Y, Hayashi M, Sakamoto M. Macrophage migration inhibitory factor-CD74 interaction regulates the expression of programmed cell death ligand 1 in melanoma cells. *Cancer Sci.* 2019;110(7):2273-83.
57. Zhao Y, Cao Y, Chen Y, Wu L, Hang H, Jiang C, et al. B2M gene expression shapes the immune landscape of lung adenocarcinoma and determines the response to immunotherapy. *Immunology.* 2021;164(3):507-23.
58. Luo M, Wang X, Wu S, Yang C, Su Q, Huang L, et al. A20 promotes colorectal cancer immune evasion by upregulating STC1 expression to block "eat-me" signal. *Signal Transduct Target Ther.* 2023;8(1):312.
59. Breitenacker K, Homolya M, Luca AC, Lang V, Trenk C, Petroczi G, et al. Down-regulation of A20 promotes immune escape of lung adenocarcinomas. *Sci Transl Med.* 2021;13(601).
60. Rossi E, Schinzari G, Zizzari IG, Maiorano BA, Pagliara MM, Sammarco MG, et al. Immunological Backbone of Uveal Melanoma: Is There a Rationale for Immunotherapy? *Cancers (Basel).* 2019;11(8).
61. Brown RAM, Richardson KL, Kabir TD, Trinder D, Ganss R, Leedman PJ. Altered Iron Metabolism and Impact in Cancer Biology, Metastasis, and Immunology. *Front Oncol.* 2020;10:476.
62. de Bruyn DP, Bongaerts M, Bonte R, Vaarwater J, Meester-Smoor MA, Verdijk RM, et al. Uveal Melanoma Patients Have a Distinct Metabolic Phenotype in Peripheral Blood. *Int J Mol Sci.*

2023;24(6).

63. Chang J, Jung HJ, Jeong SH, Kim HK, Han J, Kwon HJ. A mutation in the mitochondrial protein UQCRB promotes angiogenesis through the generation of mitochondrial reactive oxygen species. *Biochem Biophys Res Commun*. 2014;455(3-4):290-7.
64. Chang J, Jung HJ, Park HJ, Cho SW, Lee SK, Kwon HJ. Cell-permeable mitochondrial ubiquinol-cytochrome c reductase binding protein induces angiogenesis in vitro and in vivo. *Cancer Lett*. 2015;366(1):52-60.
65. Bakalian S, Marshall JC, Logan P, Faingold D, Maloney S, Di Cesare S, et al. Molecular pathways mediating liver metastasis in patients with uveal melanoma. *Clin Cancer Res*. 2008;14(4):951-6.
66. Zhang Y, Yang Y, Chen L, Zhang J. Expression analysis of genes and pathways associated with liver metastases of the uveal melanoma. *BMC Med Genet*. 2014;15:29.

## Figures

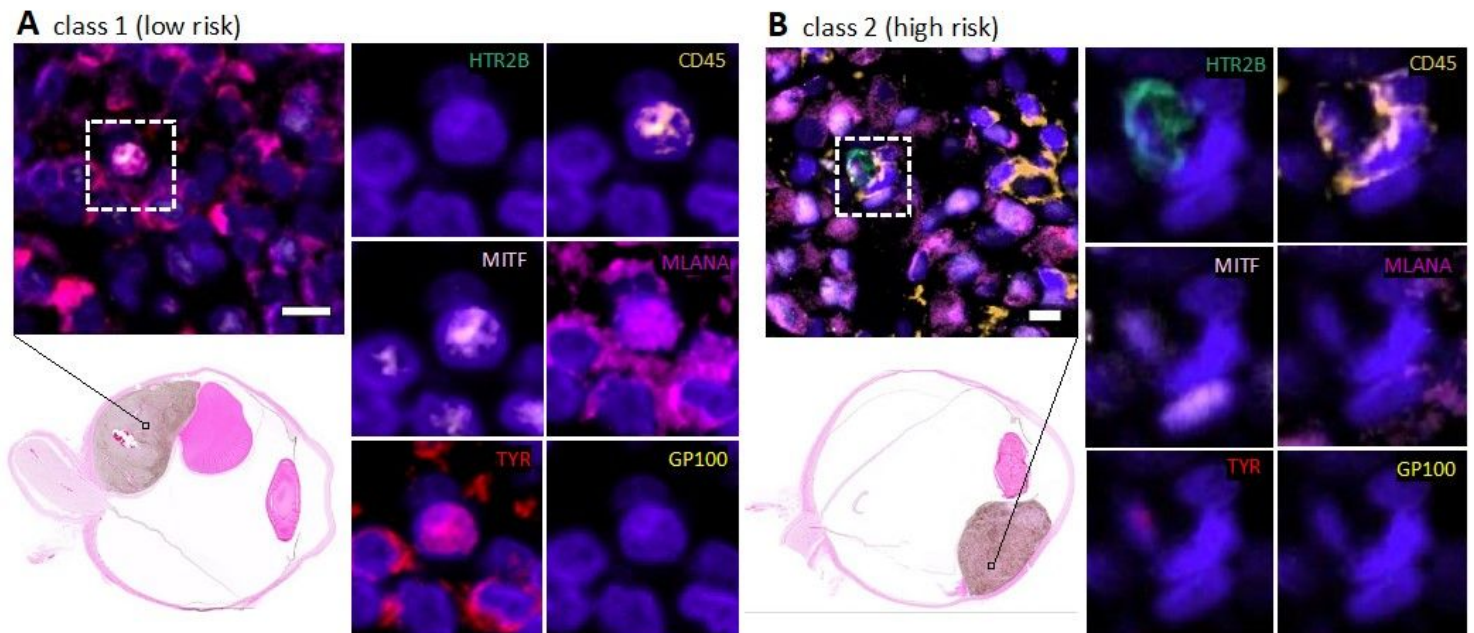


**Figure 1**

**Neoplastic-immune hybrids detected in primary UMs identified using cyCIF.** Hybrid cells identified by their co-expression of pan-leukocyte immune protein, CD45 (orange), and one or more melanocytic proteins [HTR2B (green), MITF (light pink), MLANA (magenta), Tyrosinase (red), or GP100 (yellow)]. Class 2 hybrid shows expression of HTR2B and decreased expression of tyrosinase compared to class 1 hybrid cells. Hybrid cells shown in image insets were identified in the primary tumor. H&E whole globe images for both patient samples with marked area of analyses.

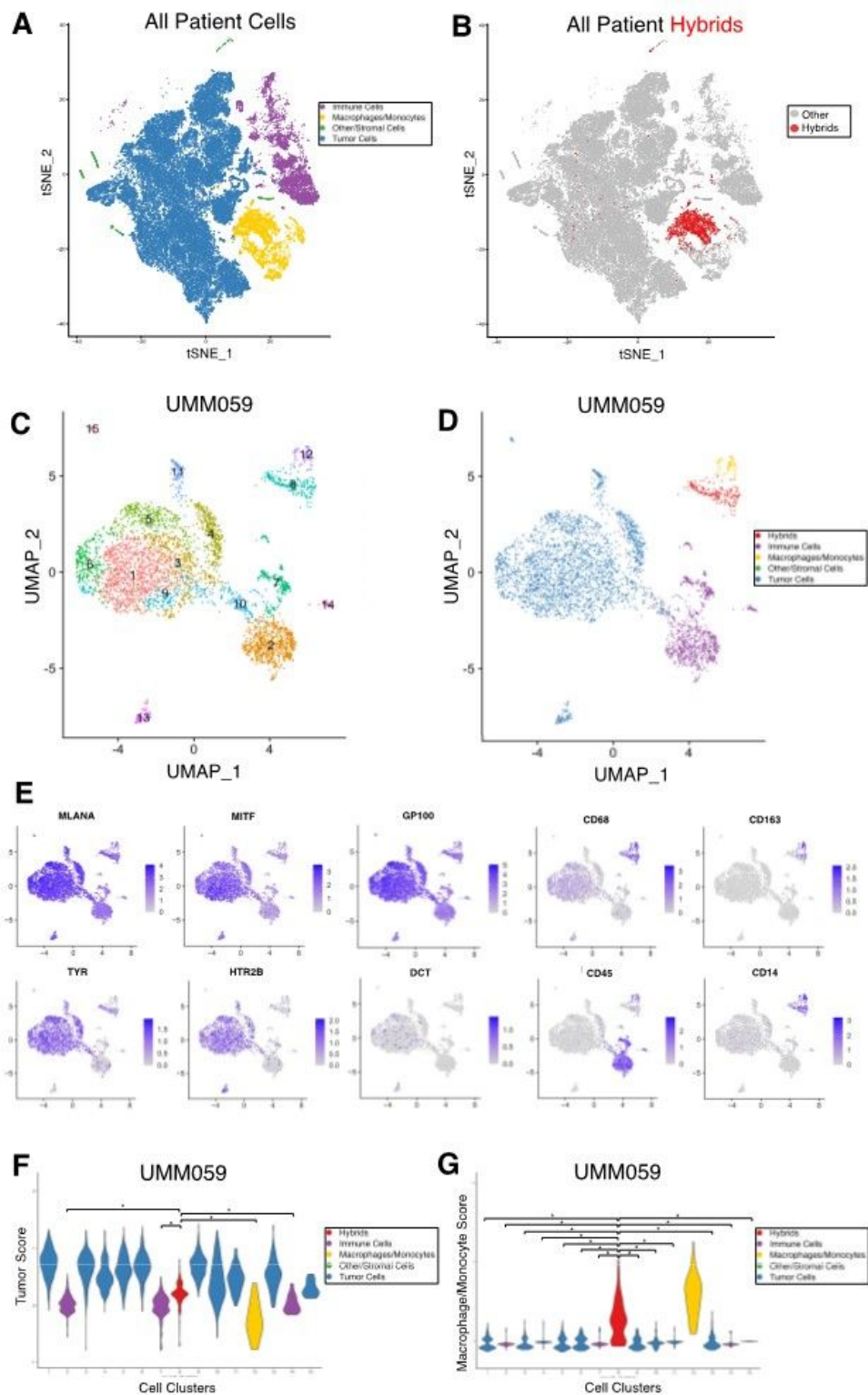


**Figure 2**

**Neoplastic-immune hybrids identified in primary UMs by scRNA-seq.** **A**) tSNE of all cells sequenced from primary tumor biopsies colored according to major cell type (tumor, macrophage/monocyte, immune, stromal/other) [13] and **B**) hybrid cells identified across all patient samples overlaid on tSNE in red. **C-G**) Hybrid analyses of scRNA-seq dataset for patient UMM059. **C**) Leiden-based clustering shown as a UMAP and annotation by major cell type in **D**) where identified hybrid cells (cluster 8) are in red. **E**) Individual

UMAPs for gene expression of melanocytic and macrophage/monocyte genes. **F, G)** Tumor score and macrophage/monocyte score violin plots for each cluster and colored according to major cell type, where hybrid cells (cluster 8, red) have significantly higher tumor scores (\* = p-value  $\leq 2 \times 10^{-8}$ . Hybrid cells (cluster 8, red) have significantly higher macrophage/monocyte scores than all other tumor cell clusters (\* = p-value  $\leq 2 \times 10^{-16}$ ). All other patient data provided in supplemental figures 2-5.

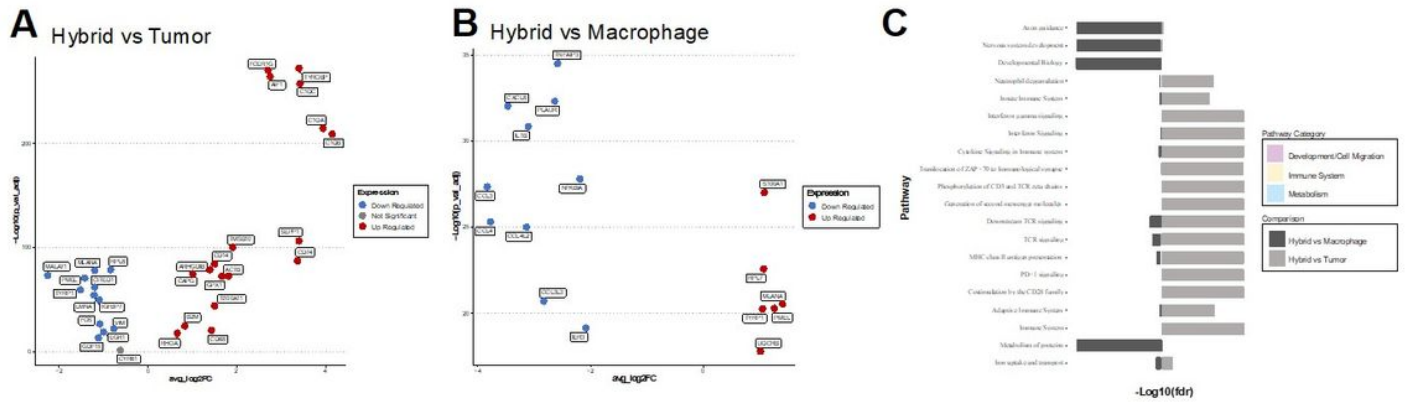


**Figure 3**

**Differential gene expression and pathway analysis for all hybrid cells compared to tumor cells and macrophages.** **A, B)** Selected significantly upregulated and downregulated genes (adjusted p-value  $\leq 0.05$  and log 2-fold change  $\geq 0.5$  or  $\leq -0.5$ ) shared across hybrid cells from all patient samples compared to tumor cells (A) and compared to macrophages (B), values shown for patient UMM059. A complete list of all differentially expressed genes for each patient sample provided in supplemental file 2. **C)** Reactome pathway enrichment analysis based on all differentially expressed genes shared across patient samples and organized by biological category, values shown for patient UMM059 and all other patient sample pathway enrichment analysis in supplemental file 3.

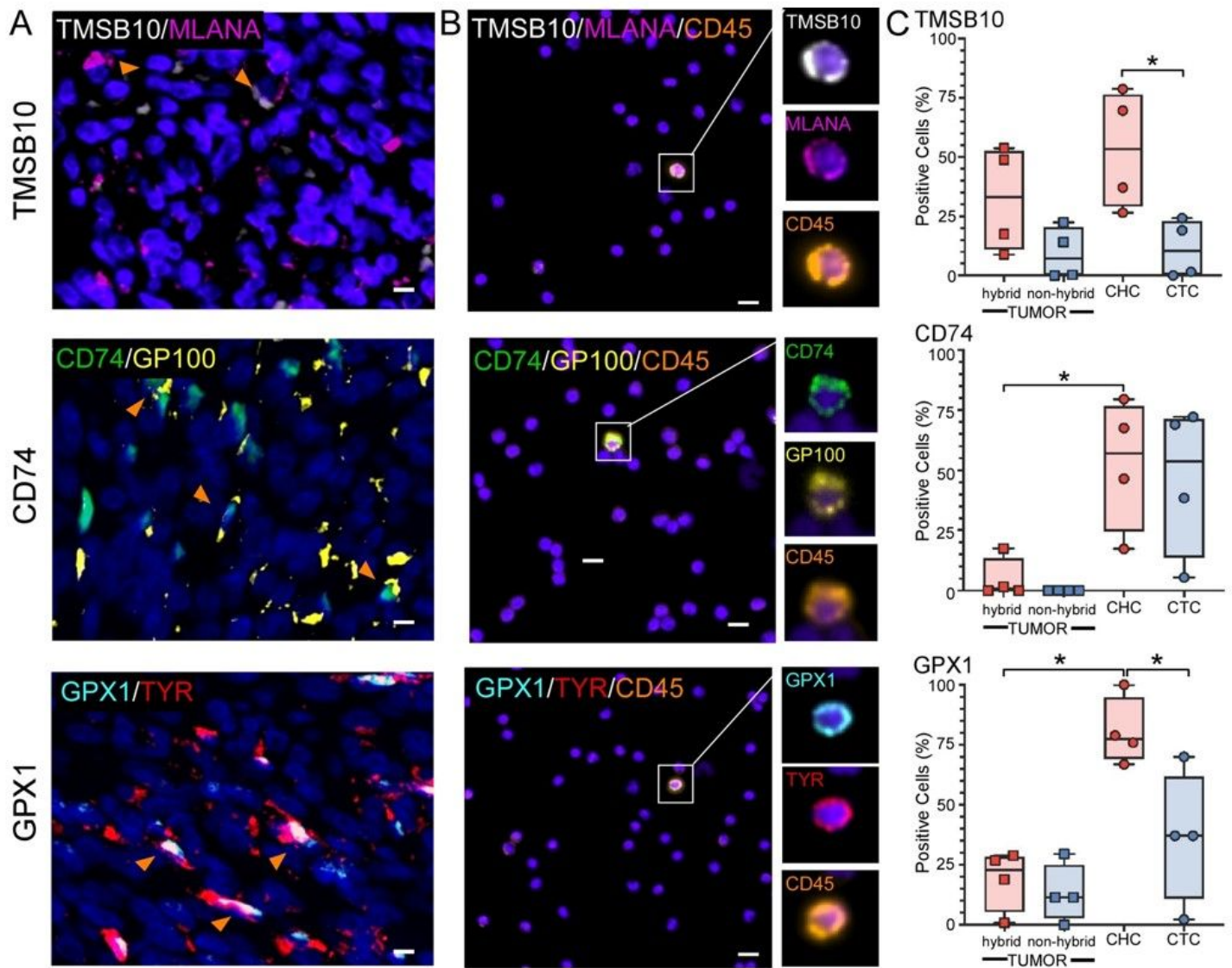
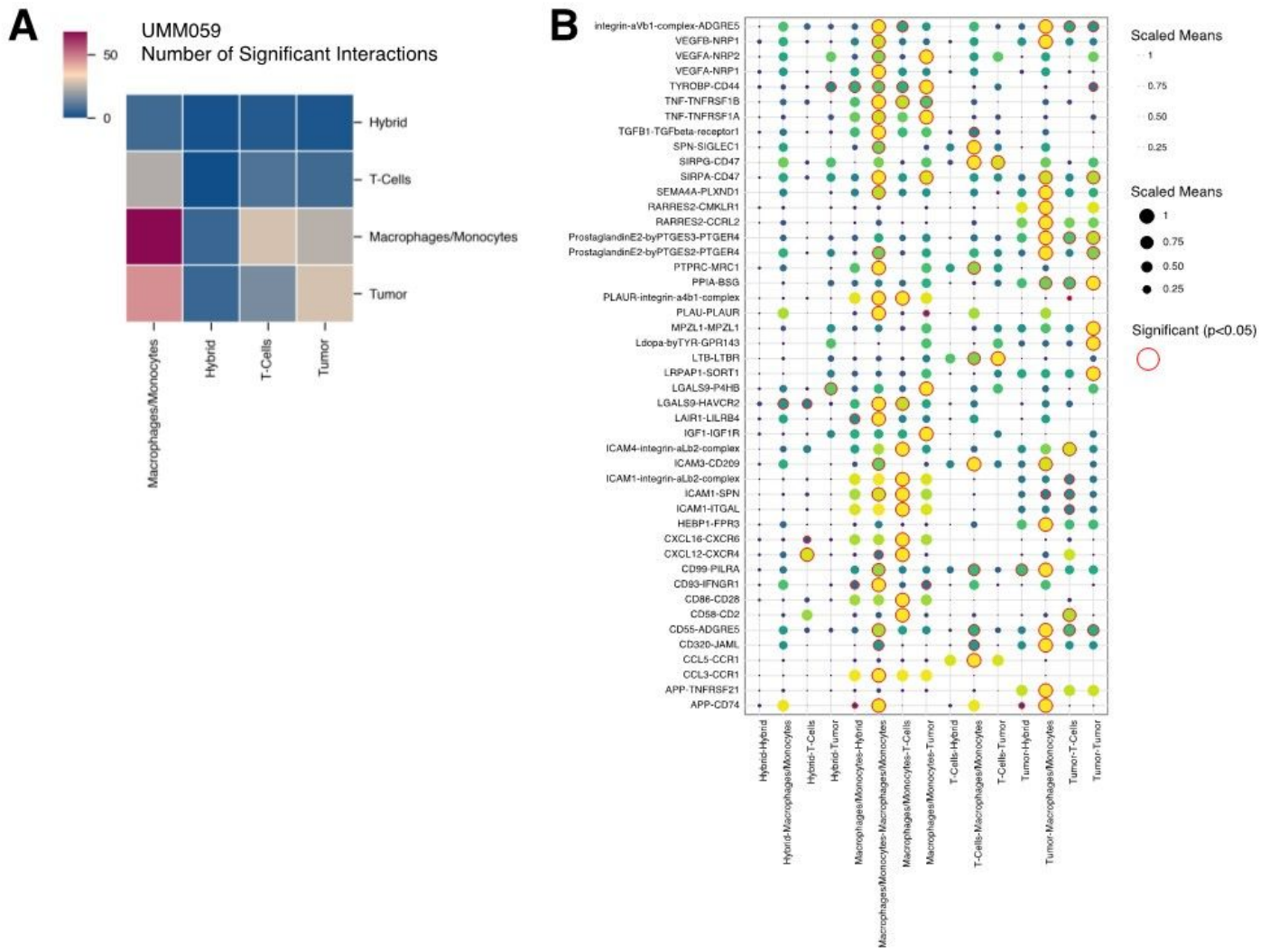


Figure 4

**Hybrid cells that successfully disseminate display upregulated expression of TMSB10, CD74 and GPX1.** Representative images of TMSB10, CD74, and GPX1 staining in **A)** primary UM tumor FFPE sections and in **B)** hybrid cells identified in circulation. **C)** The number of positive hybrid cells and tumor cells identified within primary tumor sections and peripheral blood for each biomarker, TMSB10, CD74 and GPX1, expressed as a percentage of total hybrid cells or tumor cells identified, where each dot represents 10s-10000s of cells from each individual patient sample (n=4, supplemental figure 7) (Welch's t-test, TMSB10 CHCs to CTCs p value = 0.03, CD74 tumor hybrids to CTCs p value = 0.03, GPX1 tumor hybrids to CHCs p value = 0.0007 and GPX1 CHCs to CTCs p value = 0.04, all other comparisons not significant p value > 0.05).





**Figure 5**

**Predicted ligand-receptor interactions between hybrid cells and cells of the UM tumor microenvironment.**

**A)** Heatmap showing the number of significant interactions between hybrid cells and other major cell types within the tumor microenvironment ( $p$ -value  $\leq 0.05$ ). **B)** Dot plot representing all significant ligand-receptor interactions between hybrid cells, macrophages/monocytes, tumor cells, and T-cells for patient UMM059. A complete list of significant interactions for all patient samples is included in supplemental file 4.

## Supplementary Files

This is a list of supplementary files associated with this preprint. Click to download.

- [SupplementalFigures15.pdf](#)
- [SupplementalFigure6.pdf](#)
- [SupplementalFigure7.pdf](#)

- [SupplementalFile1UMM063cluster3vs12DEGsReactomePathways.xlsx](#)
- [SupplementalFile2DEGsallpatients.xlsx](#)
- [SupplementalFile3ReactomePathwaysallpatients.csv](#)
- [SupplementalFile4CellPhoneDBallpatients.csv](#)
- [SupplementalTable12.docx](#)